Statistical Verification of Anomaly in Chiral Angle Distribution of Air-Suspended Carbon Nanotubes

AUTHOR(S):

Nishihara, Taishi; Takakura, Akira; Matsui, Keisuke; Itami, Kenichiro; Miyauchi, Yuhei

CITATION:

Nishihara, Taishi ...[et al]. Statistical Verification of Anomaly in Chiral Angle Distribution of Air-Suspended Carbon Nanotubes. Nano Letters 2022, 22(14): 5818-5824

ISSUE DATE:

2022-07-27

URL:

http://hdl.handle.net/2433/276862

NANO LETTERS

pubs.acs.org/NanoLett Letter

Statistical Verification of Anomaly in Chiral Angle Distribution of Air-Suspended Carbon Nanotubes

Taishi Nishihara,* Akira Takakura, Keisuke Matsui, Kenichiro Itami, and Yuhei Miyauchi*

Cite This: *Nano Lett.* 2022, 22, 5818−5824 Read Online

ACCESS | Metrics & More | Article Recommendations | Supporting Information

ABSTRACT: Single-walled carbon nanotubes (SWCNT) have long attracted attention due to their distinct physical properties, depending on their chiral structures (chiralities). Clarifying their growth mechanism is important toward perfect chirality-controlled bulk synthesis. Although a correlation between the chirality distribution and the carbon atom configuration at an open tube edge has been predicted theoretically, lack of sufficient statistical data on metallic and semiconducting SWCNTs prohibited its verification. Here, we report statistical verification of the chirality distribution of 413 as-grown individual air-suspended SWCNTs with a length of over 20 μm using broadband Rayleigh spectroscopy. After excluding the impact of the difference in the number of possible SWCNT structures per chiral angle interval, the abundance profile with chiral angle exhibits an increasing trend with a distinct anomaly at a chiral angle of approximately 20°. These results are well explained considering the growth rate depending on armchair-shaped site configurations at the catalyst−nanotube interface.

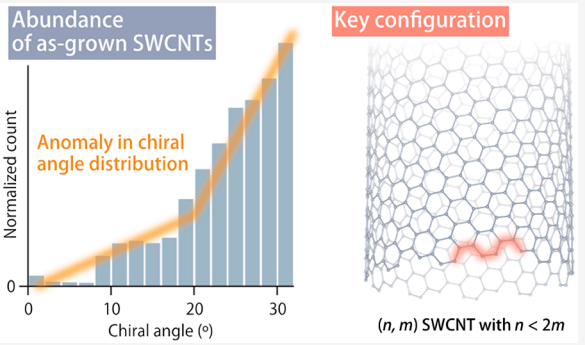

KEYWORDS: *carbon nanotubes, Rayleigh spectroscopy, chirality, armchair, CVD growth*

Carbon nanotubes[1] have attracted attention due to their district physical properties, for example, strong light−matter interaction,[2] high electrical[3,4] and thermal conductivity,[5,6] high thermal stability,[7,8] and outstanding strength-to-weight ratio.[9,10] In addition, their potential to be generated from carbon dioxide has recently expanded their importance in terms of social demand to reduce carbon dioxide emissions on a global scale. Among carbon nanotubes, single-walled carbon nanotubes[11] (SWCNT) have excellent properties that depend on their chiral structures, which are specified by pairs of a diameter d and chiral angle θ (Figure 1a) or by chiral indices (n,m) (Figure 1b). Even when SWCNTs have similar diameters and chiral angles, they may be metallic ($n - m = 3q$; q is an integer) or semiconducting ($n - m \neq 3q$)[12−14] with different optical transition energies originating from exciton resonances.[15−18] The structure-dependent narrow-window exciton resonance provides a promising application as a wavelength-selective near-infrared-to-visible photon emitter.[8,19−21] In addition, even the mechanical strength of SWCNTs, whose strength-to-weight ratio is among the highest among known materials, depends on the chiral structures of the SWCNTs.[10,22] The preferred structure of SWCNTs depends on the applications; thus, structure-controlled synthesis of SWCNTs has attracted attention in a wide range of scientific fields.[23−43]

To date, various methods that can generate a small amount of highly structure-controlled SWCNTs have been reported,[23−33] and mechanisms to explain the structure selectivity have been proposed.[34−41] Bulk synthesis of much narrower chirality distribution has been reported recently;[42,43] however, bulk synthesis of perfectly structure-controlled SWCNTs has not yet been achieved, and deeper understanding of the growth mechanism is required to realize this goal. Previous experimental studies have reported the preferential growth of SWCNTs with large chiral angles (red region in Figure 1b), referred to as armchair (achiral, with θ = 30°) and near-armchair (chiral, with $\theta \sim 30°$) SWCNTs, in as-grown condition.[23,40,41,44−47] This abundant growth has been verified by theoretical calculations, and the abundant armchair sites on the open tube edge (red and blue squares in Figure 1a) with a smaller potential barrier for carbon adhesion than the zigzag sites (black circles in Figure 1a) have been suggested as the primary origin of this preferential growth.[35,37] In addition, for the solid catalyst case, theoretical studies have predicted the preferential growth of near-armchair SWCNTs over armchair SWCNTs due to the existence of kink edges (indicated by the black dotted line in Figure 1a) that promote screw dislocation[34,36] or the larger entropy of atom configurations

Received: April 12, 2022
Revised: July 2, 2022
Published: July 8, 2022

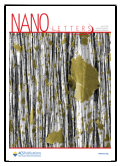

https://doi.org/10.1021/acs.nanolett.2c01473
Nano Lett. 2022, 22, 5818−5824

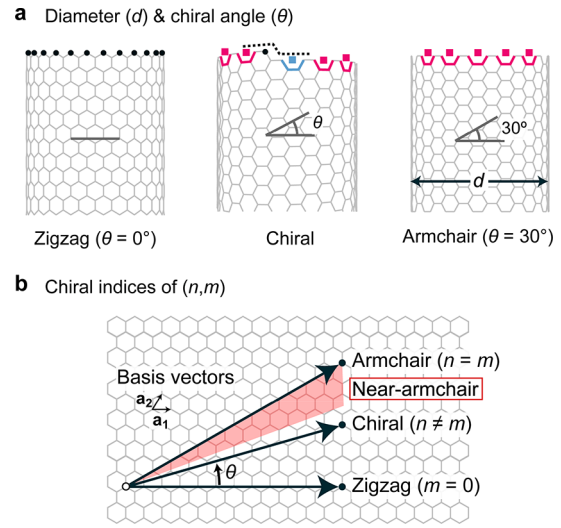

Figure 1. Structural classification of single-walled carbon nanotubes. (a) Definitions of diameter (d) and chiral angle (θ). The chiral angle is defined as the angle between the zigzag direction and the circumference (θ = 0°−30°). Black circles indicate carbon atoms composing zigzag sites. Squares indicate pairs of carbon atoms composing armchair sites. The black dotted line indicates a kink edge. (b) Definition of chiral indices of (n,m). The chiral indices of (n,m) represent the chiral vector (black arrows) of a nanotube mapped on a graphene plane with a basis of $\mathbf{a}_1$ and $\mathbf{a}_2$.

of edge structures.[37] In contrast, for the liquid catalyst case the preferential growth of achiral armchair species has been predicted because the energy costs of the edge nucleation of each structure are comparable, and the number of armchair sites becomes the dominant factor in the growth.[36] Thus, the structure abundance distribution as a function of θ includes the information about the catalyst phase (solid or liquid), as well as the dependence of the growth rate on the overall atom configurations of the edge structures, which is most important in terms of experimental verification of the theoretical predictions. However, the correlation between the statistical abundance distribution and the structure-dependent edge configurations has remained to be clarified thoroughly from an experimental perspective.

Here, we report the statistical structure distribution of individual air-suspended SWCNTs grown by alcohol chemical vapor deposition (CVD). For simplicity, we studied as-grown isolated individual SWCNTs suspended over a slit because SWCNT bundling and/or interactions with the substrate may complicate their growth process and structural selectivity. We determined the chiral structure of 413 SWCNTs via broadband Rayleigh spectroscopy, covering photon energies in the range of 0.8−2.8 eV, which enabled rapid and efficient structure characterization of both semiconducting and metallic SWCNTs. The preferential growth of SWCNTs with large chiral angles was observed, together with inhibited growth of SWCNTs with small chiral angles with diameters above ∼2.6 nm. Statistical analyses revealed that the abundance distribution exhibited an increasing trend with an anomaly in the derivative at the chiral angle of approximately 20°. In addition, the growth of achiral armchair SWCNTs was preferential to that of chiral near-armchair species. We demonstrate that the anomaly in the abundance distribution can be accounted for by considering the different contributions of open tube edge structures to the SWCNT growth rate.

SWCNTs were grown and suspended over open slits (width, 20−30 μm) prepared at the center of silicon substrates via ambient CVD[48] using a modified fast-heating process[49,50] (growth temperature, 900 °C; see Methods for details). Their structures were determined by Rayleigh spectroscopy,[2,45,51,52] which is applicable to structure characterization of both semiconducting and metallic SWCNTs. All SWCNTs have inherent sets of multiple optical transitions originating from exciton resonances in each one-dimensional sub-band, which are widely distributed across the infrared-to-visible photon energy range. In this study, we applied Rayleigh spectroscopy in the broad photon energy range of 0.8−2.8 eV (broadband Rayleigh spectroscopy[8,10]), where a sufficient number of exciton resonance peaks to specify the structure is included (Figure 2a; see Methods for details). The observed exciton series in the 0.8−2.8 eV range were compared to an empirical table developed to represent the relationship between the nanotube structure and set of optical transition energies,[52] leading to rapid structure characterization (see Supporting Information Note for details). In the experiments, as-grown suspended SWCNTs were searched under white light illumination (Figure 2b) followed by broadband Rayleigh spectroscopy.

We determined the chiral structure of 413 SWCNTs, including 276 semiconducting SWCNTs and 137 metallic SWCNTs. Assuming a random distribution of SWCNT chiral structures, one-third of the SWCNTs should have been metallic. Although the results revealed a ratio of nearly 2:1 for semiconducting and metallic SWCNTs, the chiral structure distribution demonstrated preferential regions with a characteristic diameter and chiral angle (Figures 2c). SWCNTs with d = 1−3 nm and large chiral angles (near-armchair types) were preferential. In contrast, relatively small-diameter SWCNTs (d < ∼1 nm) and near-zigzag and zigzag SWCNTs (θ < ∼10°) with d > ∼ 2.6 nm were hardly found under these growth conditions. Figure 2d,e shows chiral structure distribution as a function of diameter and chiral angle, respectively, where the bin sizes are 0.2 nm and 2°, respectively. In Figure 2e, the dark red bar at 30° represents the number of only armchair SWCNTs although it is plotted with the same bin size as the other SWCNTs. As shown in Figure 2d, the average diameter was 2.22 nm (standard deviation: 0.52 nm), which is greater than that reported in previous studies (d = ∼1 nm).[23,44,46] This is because the growth temperature was higher than in those studies.[23,44,46] A similar abundance to ours was reported for a similar growth temperature.[45] Despite the difference in preferential diameters, both our results and those of previous studies[23,44−46] demonstrate that as-grown SWCNTs favors large chiral angles (Figure 2e). In addition, in our experiment 18 armchair SWCNTs were detected (their spectra are shown in the inset of Figure 2c).

To investigate the chiral angle dependence of the fractional abundance, we analyzed the data of the SWCNTs with their diameters falling within one standard deviation of the mean (d = 1.70−2.74 nm; Figure 3a). Here, the bin size is 2°, and the red bar at 30° represents the number of armchair SWCNTs with the same bin size. We compared this distribution to the theoretically expected distribution under the fully random growth condition, where each (n,m) SWCNT was assumed to grow with equal probability. To calculate the theoretical distribution under the random growth condition, first we counted possible numbers N_R (θ) of chiral indices (n,m) within the diameter range of d = 1.70−2.74 nm in each bin of

https://doi.org/10.1021/acs.nanolett.2c01473
Nano Lett. 2022, 22, 5818−5824

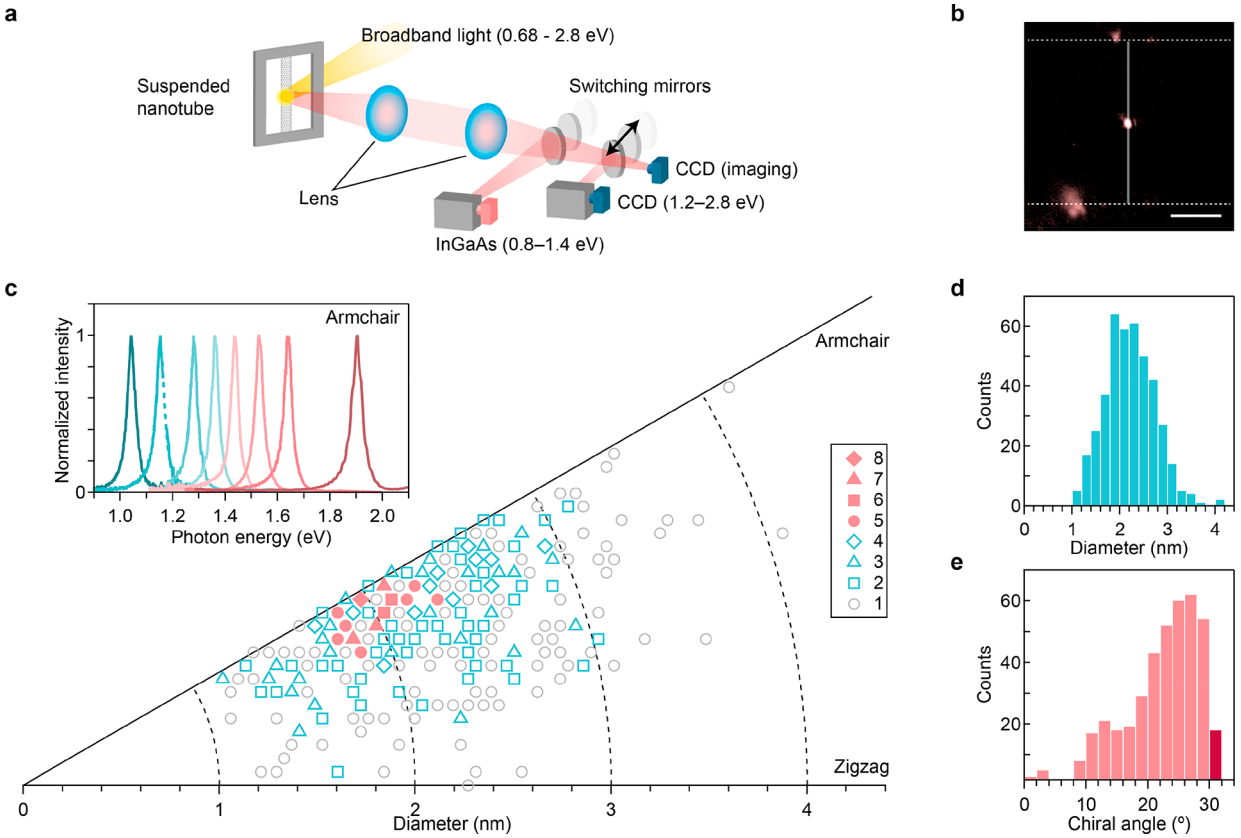

Figure 2. Structure distribution of individual as-grown SWCNTs. (a) Schematic of the optical setup for broadband Rayleigh spectroscopy. Switching mirrors change the optical paths to the charge-coupled device (CCD) camera for imaging, to the CCD camera for spectroscopy, or to the indium−gallium−arsenide (InGaAs) camera for spectroscopy. (b) Optical image of an individual SWCNT. The white vertical line and horizontal dotted lines indicate the positions of the SWCNT and slit edges, respectively. The bright spot at the center indicates the point at which the broadband light is focused. Scale bar: 10 μm. The color is modified for clarity. (c) Structure distribution in a polar plot of the diameter and chiral angle. Each marker indicates the number of corresponding SWCNTs. The inset shows the Rayleigh spectra of (n,n) armchair SWCNTs of the first sub-band exciton resonance peaks (n = 10, 12−16, 18, 20). (d,e) Structure distribution as a function of (d) diameter and (e) chiral angle. The bin sizes are 0.2 nm and 2°, respectively. The dark red bar at 30° in (e) represents the number of only armchair SWCNTs plotted with the same bin size as the other SWCNTs.

Figure 3a. Then, the probability of finding SWCNTs having a chiral angle of within $\theta \pm 1°$ was calculated as $P_R(\theta) = N_R(\theta)/\sum N_R(\theta)$, where $\sum N_R(\theta)$ is the total number for all θ. Note that chiral SWCNTs have an equal number of left- and right-handed enantiomeric helical forms[53−56] (Figure 3a, inset) but they were indistinguishable in this study because we did not measure Rayleigh scattering circular dichroism[56] to distinguish enantiomeric helical forms. Thus, the expected number of each chiral SWCNT was two times greater than that of the achiral species. The expected value under the random growth condition denoted as $\langle N_R(\theta)\rangle$ is given as follows

$$\langle N_R(\theta)\rangle = \left(\sum N(\theta)\right) \times P_R(\theta) \quad (1)$$

where $N(\theta)$ is the number of experimentally found SWCNTs within $\theta \pm 1°$, and $\sum N(\theta)$ is the total number for all θ in the experiment. Recall that only armchair SWCNTs were counted independently. The green markers in Figure 3a indicate $\langle N_R(\theta)\rangle$ with a 95% confidence interval estimated from the Poisson distribution (orange band). A comparison of the experimental and expected values indicated that the abundance distribution of SWCNTs could be divided qualitatively into three groups, that is, SWCNTs with $\theta < \sim 10°$, $\sim 10° < \theta < \sim 20°$, and $\sim 20° < \theta$ (referred to as small-, middle-, and large-chiral-angle SWCNTs, respectively). Compared to the middle-chiral-angle SWCNTs, which exhibited moderate deviation, the experimental number of small- and large-chiral-angle SWCNTs deviated greatly from the expected range under the random growth condition (orange band). The abundance of large-chiral-angle SWCNTs exceeded the upper limit of the expected range (orange band) considerably, and the abundance of small-chiral-angle species was significantly less than the expected minimum value. Thus, stochastically, these results confirm the preferential growth of large-chiral-angle SWCNTs, including both near-armchair and armchair SWCNTs. To further discuss the prevalence of large-chiral-angle SWCNTs, Figure 3b plots the normalized count $N(\theta)/\langle N_R(\theta)\rangle$, excluding the impact of the difference in the number of possible SWCNT structures in each bin. As shown in Figure 3b, the normalized abundance distribution clearly displays preferential growth of armchair SWCNTs, although these SWCNTs were apparently the least abundant among SWCNTs with large chiral angles, as shown in Figures 2e and 3a.

In the following, we discuss the practical implications of the results on the growth mechanism. A previous theoretical study[36] predicted a significant impact of the morphology of the open tube edge at the nanotube-metal catalyst particle interface on the growth of SWCNTs. The fractional abundance

https://doi.org/10.1021/acs.nanolett.2c01473
Nano Lett. 2022, 22, 5818−5824

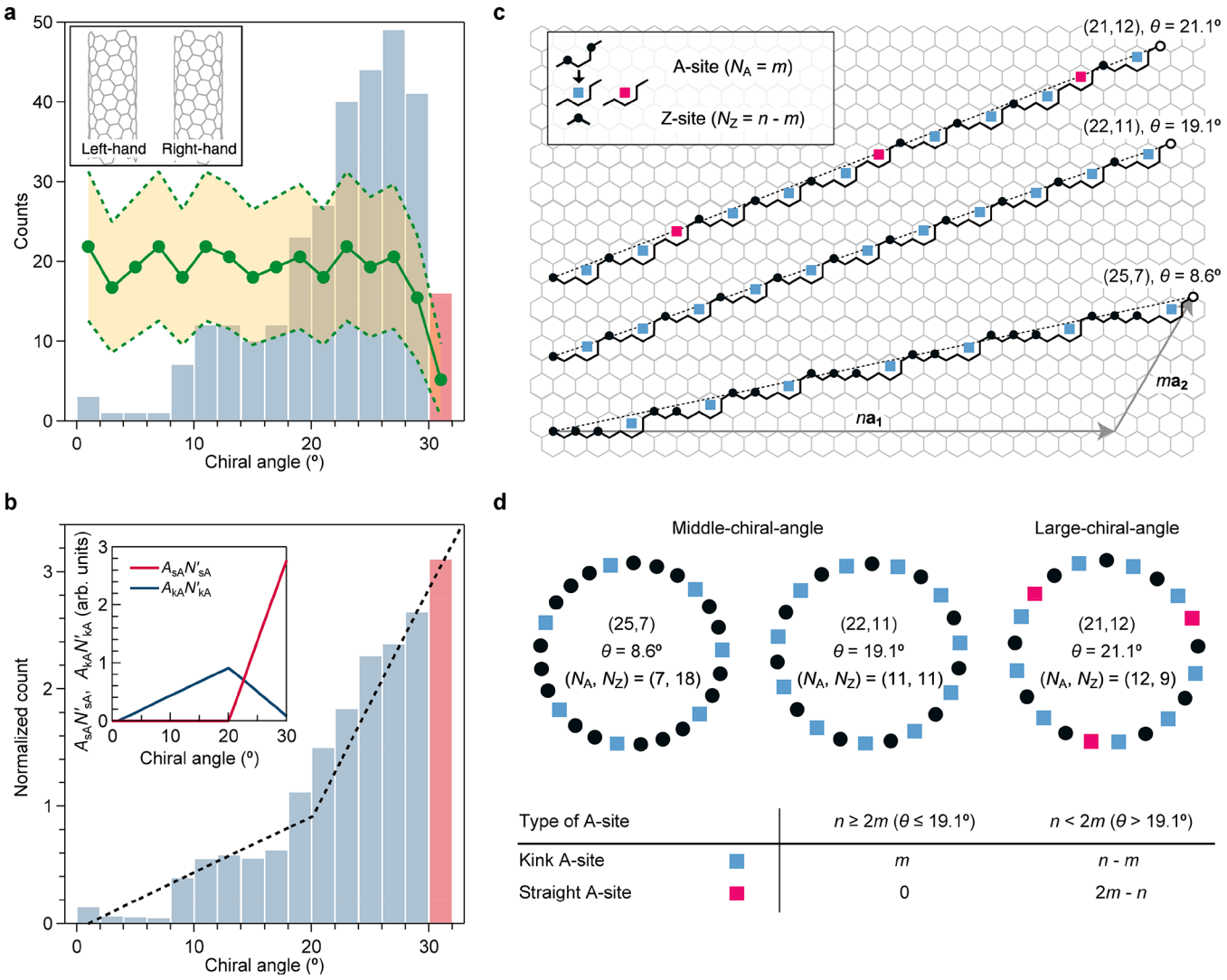

Figure 3. Chiral angle dependence of structure distribution. (a) Histogram of SWCNTs with diameters of 1.70−2.74 nm as a function of the chiral angle. Bin size, 2°. The red bar at 30° represents the number of armchair SWCNTs with the same bin size. Green markers show the number of SWCNTs expected under the random growth condition with 95% confidence interval estimated from the Poisson distribution (orange band). The inset shows an example of enantiomers of the (8,4) SWCNT. (b) Histogram of the normalized count. The black dotted line represents the fitting result. The inset shows the growth contributed to by straight armchair sites (A-sites; $A_{sA}N'_{sA}$) and kink A-sites ($A_{kA}N'_{kA}$). (c) Open tube edges of (25,7), (22,11), and (21,12) SWCNTs projected onto graphene plane (solid black lines). Dotted lines represent open tube edges with the minimal circle length. As shown in the inset, red and blue squares and black circles indicate A-sites and zigzag sites (Z-sites), respectively, and their numbers are indicated by N_A and N_Z. (d) Open tube edges represented using A-sites and Z-sites (upper panel). Summary of the number of consecutive and isolated A-sites for a (n,m) SWCNT (bottom panel).

of each SWCNT type was expected to be proportional to the product of the nucleation probability $P_{n,m}$ and growth rate $\Gamma_{n,m}$, both of which depend on the chiral angle.[36] The growth rate $\Gamma_{n,m}$ depends on whether the catalyst is solid ($\Gamma_{n,m} \propto 30° - \theta$) or liquid ($\Gamma_{n,m} \propto \theta$).[36] Thus, the key experimental result differentiating the two cases is the preferential growth of the armchair SWCNTs over other structures, which is allowed only for the liquid state catalyst case[38] and observed in this study. Therefore, our experimental condition could be described as the liquid catalyst case, where nearly random nucleation of the open tube edge was expected. This situation allowed us to focus on the impact of growth rate $\Gamma_{n,m}$ on the abundance distribution.

Thus, the most naive prediction of the abundance distribution for the liquid catalyst case is that it is proportional to the chiral angle θ due to $\Gamma_{n,m} \propto \theta$.[36] However, the experimental result shown in Figure 3b clearly exhibits an abruptly accelerating increasing trend as a function of θ, where the slope for SWCNTs with $\theta > \sim 20°$ is much steeper than that for SWCNTs with $\theta < \sim 20°$. To further explore the implications of this anomalous trend, we considered the geometry of the open tube edges by referencing a previous study.[40] Figure 3c shows the open tube edges projected on a graphene plane for middle- and large-chiral-angle SWCNTs with similar diameters of ∼2.28 nm. Here, the geometry for the minimal-length circle along the nanotube circumference is considered for simplicity. As shown in the inset of Figure 3c, the squares indicate pairs of carbon atoms composing the armchair sites (A-sites), and the black circles indicate zigzag sites (Z-sites). The number of A-sites (N_A) and Z-sites (N_Z) is represented as $N_A = m$ and $N_Z = n - m$, respectively (see the (25,7) SWCNT for an example).[35] For medium-chiral-angle

https://doi.org/10.1021/acs.nanolett.2c01473
Nano Lett. 2022, 22, 5818−5824

(25,7) and (22,11) SWCNTs, only isolated A-sites (blue squares) are evident, which form kinks at the open tube edge. In contrast, the large-chiral-angle (21,12) SWCNT has consecutive A-sites forming partially straight open tube edges (adjacent blue and red squares). This is more apparent in the schematic representation of the open tube edges as A-sites and Z-sites in the upper panel of Figure 3d. Note that N_A is less than N_Z for middle-chiral-angle SWCNTs; thus, all A-sites are isolated. For example, for the (22,11) SWCNT, the A-sites and Z-sites alternate in a row because $N_A = N_Z$. In contrast, for large-chiral-angle SWCNTs, consecutive A-sites always exist because N_A was greater than N_Z.

According to this geometric analysis, here we divide A-sites into two groups, that is, A-sites that form kinks (blue squares adjacent to a Z-site on the left; referred to as a kink A-site) and those forming a straight edge at the open tube edge (red squares adjacent to an A-site on the left; referred to as a straight A-site). The number of kink A-sites (N_{kA}) is given by N_A if $n \geq 2m$ and N_Z if $n < 2m$, that is, m or $n - m$. The number of straight A-sites (N_{sA}) is given by $N_{sA} = N_A - N_{kA}$; thus, it is zero if $n \geq 2m$ or $2m - n$ if $n < 2m$ (summarized in the bottom panel of Figure 3d). We phenomenologically relate the SWCNT fractional abundance to the number of A-sites as follows

$$N(\theta)/\langle N_R(\theta)\rangle = A_{sA}N'_{sA}(\theta) + A_{kA}N'_{kA}(\theta) \quad (2)$$

where $A_{s(k)A}$ is the contribution from the straight (kink) A-sites, and $N'_{s(k)A}$ is the density of the straight (kink) A-sites, which is given by $N'_{s(k)A} = N_{s(k)A}/\pi d$. The chiral angle θ is related to the chiral indices (n,m) by

$$\theta = \sin^{-1}\left(\sqrt{3}m/2\sqrt{n^2 + m^2 + nm}\right)$$

Here, we neglected the contribution from zigzag sites due to our observations and a previous report on the larger potential barrier for carbon adhesion in zigzag sites than in armchair sites.[35] The best fit (dotted line in Figure 3b) well reproduced the abruptly accelerating trend above $\theta \sim 20°$. The inset of Figure 3b shows the details of the relative contribution of the $A_{sA}N'_{sA}$ and $A_{kA}N'_{kA}$ terms to the fluctional abundance. The ratio of $A_{sA}/A_{kA} = 2.2$ obtained by the fit suggests that the existence of the straight A-sites contributed to the growth rate approximately two times more than the existence of kink A-sites. Thus, the experimentally observed anomaly in the abundance distribution is a signature of the geometry-dependent contribution of the nanotube edge to the growth rate. Finally, we briefly comment on the step like feature found in the chiral angle distribution around $\theta \sim 8°$ (Figure 3b) that deviates from the linear change expected from eq 2. Possible reasons for this could be that the near zigzag SWCNTs with slow growth rate could not be detected due to their shorter lengths than the open slit width on our substrates (see Methods), or there might be any unknown intrinsic mechanism. This topic remains as a future issue.

In this study, we investigated the chirality distribution of individual as-grown SWCNTs using broadband Rayleigh scattering spectroscopy. The chirality distribution of 413 observed SWCNTs revealed the preferential growth of armchair and near-armchair SWCNTs. Among large-chiral-angle SWCNTs, the preferential growth of armchair SWCNTs was confirmed statistically. The obtained abundance distribution exhibited an increasing trend with an anomaly at a chiral angle $\theta \sim 20°$. We found that the experimental trend, including the chiral angle where the anomaly occurs, can be well explained as a consequence of the different contributions of consecutive and isolated A-sites on the open tube edge to the growth. These findings on the anomalous abundance distribution and the proposed model accounting for the chiral angle dependence of the growth rate are expected to allow us to obtain deeper understanding of the growth mechanism of SWCNTs.

METHODS

Synthesis of Suspended SWCNTs. SWCNTs were grown using the CVD method with cobalt (Co)- and molybdenum (Mo)-doped mesoporous silica catalysts on a SiO_2/Si substrate with an open slit of 20−30 μm on the basis of ref 49. The catalysts were prepared as follows. A mesoporous silica solution was prepared by mixing tetraethoxysilane, 0.1 M HCl, and dehydrated ethanol in a volume ratio of 2:1:12 at 70 °C for 1 h. Co acetate tetrahydrate and Mo acetate dimer were dissolved in dehydrated ethanol with 8 wt % surfactant (Pluronic F127) with a moderate bath sonicator for 1 h such that the concentration of each metallic species was 0.2 and 0.1 wt %, respectively. The mesoporous silica solution and catalyst solution were then mixed in equal volume ratio and concentrated to half of the initial volume. CVD growth was performed as follows. The catalysts were placed at a distance of approximately 20 μm from the slits of the substrates. The substrates were heated at 400 °C for 15 min in a dry air flow at 400 standard cubic centimeters per minute (sccm) to calcine the catalysts. The CVD chamber was cooled to room temperature and evacuated to a pressure of <1 Pa. Argon−hydrogen (Ar−H_2) mixture gas (3% H_2) and ethanol were used as the carrier gas and carbon feedstock, respectively. The Ar−H_2 gas bubbled into ethanol was introduced into the CVD chamber at 100 sccm together with the Ar−H_2 gas flow at 400 sccm. The substrates were heated rapidly to 900 °C, and CVD growth was performed for 15 min. Then, the CVD chamber was cooled to room temperature with the Ar−H_2 gas at a flow rate of 400 sccm.

Broadband Rayleigh Spectroscopy. Broadband light produced by a supercontinuum source (Fianium, WL-SC-400-PP-4 or YSL photonics, SC-Pro) was focused on an individual SWCNT placed in a vacuum chamber. The integrated power was approximately 2 mW over photon energies of 0.56−2.8 eV. The scattered light collected by an objective lens (numerical aperture: 0.42) was detected by three types of detectors that were remotely switchable by mirrors (Figure 2a). Following observation of the SWCNT image through a charge-coupled device (CCD) camera (Watec, WAT-910HX/RC), the Rayleigh spectra were measured using a monochromator with a thermoelectrically cooled CCD camera (Princeton Instruments, ProEM) and a monochromator with an indium−gallium−arsenide (InGaAs) two-dimensional photodiode array (Princeton Instruments, NIRvana).

ASSOCIATED CONTENT

Supporting Information

The Supporting Information is available free of charge at https://pubs.acs.org/doi/10.1021/acs.nanolett.2c01473.

Details of structure assignment scheme using broadband Rayleigh scattering spectroscopy; comparison of the structure assignment scheme by the broadband Rayleigh (0.8−2.8 eV) spectroscopy with that relying on the

https://doi.org/10.1021/acs.nanolett.2c01473
Nano Lett. 2022, 22, 5818−5824

combination of Rayleigh (1.2−2.8 eV) and Raman spectroscopies, broadband Rayleigh scattering spectra of (15,13), (13,13), and (9,8) SWCNTs (PDF)

AUTHOR INFORMATION

Corresponding Authors

Yuhei Miyauchi − *JST-ERATO, Itami Molecular Nanocarbon Project, Nagoya University, Chikusa, Nagoya 464-8602, Japan; Graduate School of Science, Nagoya University, Chikusa, Nagoya 464-8602, Japan; Institute of Advanced Energy, Kyoto University, Uji, Kyoto 611-0011, Japan;* orcid.org/0000-0002-0945-0265; Email: miyauchi@iae.kyoto-u.ac.jp

Taishi Nishihara − *JST-ERATO, Itami Molecular Nanocarbon Project, Nagoya University, Chikusa, Nagoya 464-8602, Japan; Graduate School of Science, Nagoya University, Chikusa, Nagoya 464-8602, Japan; Institute of Advanced Energy, Kyoto University, Uji, Kyoto 611-0011, Japan;* orcid.org/0000-0001-6973-2005; Email: nishihara.taishi.8x@kyoto-u.ac.jp

Authors

Akira Takakura − *JST-ERATO, Itami Molecular Nanocarbon Project, Nagoya University, Chikusa, Nagoya 464-8602, Japan; Graduate School of Science, Nagoya University, Chikusa, Nagoya 464-8602, Japan; Institute of Advanced Energy, Kyoto University, Uji, Kyoto 611-0011, Japan*

Keisuke Matsui − *JST-ERATO, Itami Molecular Nanocarbon Project, Nagoya University, Chikusa, Nagoya 464-8602, Japan; Graduate School of Science, Nagoya University, Chikusa, Nagoya 464-8602, Japan*

Kenichiro Itami − *JST-ERATO, Itami Molecular Nanocarbon Project, Nagoya University, Chikusa, Nagoya 464-8602, Japan; Graduate School of Science and Institute of Transformative Bio-Molecules (WPI-ITbM), Nagoya University, Chikusa, Nagoya 464-8602, Japan;* orcid.org/0000-0001-5227-7894

Complete contact information is available at: https://pubs.acs.org/10.1021/acs.nanolett.2c01473

Author Contributions

T.N. and Y.M. conceived the concept, and K.I. directed the project. A.T. fabricated the SWCNT synthesis apparatus, and A.T. and K.M. synthesized the SWCNTs. T.N. arranged the optical setup, and T.N. and Y.M. considered the structure assignment scheme. T.N., A.T., and K.M. carried out the optical experiments and determined the SWCNT structures. T.N. and Y.M. considered the growth mechanism. All the authors contributed to writing the manuscript.

Notes

The authors declare no competing financial interest.

ACKNOWLEDGMENTS

This work was supported by the ERATO program from JST (K.I.) (Grant JPMJER1302). Part of this work was supported by JST CREST Grant JPMJCR18I5 (Y.M.), JSPS KAKENHI Grant JP24681031 (Y.M.), and JP19K15384, JP21K14486 (T.N.).

REFERENCES

(1) Iijima, S. Helical Microtubules of Graphitic Carbon. *Nature* **1991**, *354*, 56−58.
(2) Sfeir, M. Y.; Beetz, T.; Wang, F.; Huang, L.; Huang, X. M. H.; Huang, M.; Hone, J.; O'Brien, S.; Misewich, J. A.; Heinz, T. F.; Wu, L.; Zhu, Y.; Brus, L. E. Optical Spectroscopy of Individual Single-Walled Carbon Nanotubes of Defined Chiral Structure. *Science* **2006**, *312*, 554−556.
(3) Dai, H.; Wong, E. W.; Lieber, C. M. Probing Electrical Transport in Nanomaterials: Conductivity of Individual Carbon Nanotubes. *Science* **1996**, *272*, 523−526.
(4) Tans, S. J.; Devoret, M. H.; Dai, H.; Thess, A.; Smalley, R. E.; Geerligs, L. J.; Dekker, C. Individual Single-Wall Carbon Nanotubes as Quantum Wires. *Nature* **1997**, *386*, 474−477.
(5) Yu, C.; Shi, L.; Yao, Z.; Li, D.; Majumdar, A. Thermal Conductance and Thermopower of an Individual Single-Wall Carbon Nanotube. *Nano Lett.* **2005**, *5*, 1842−1846.
(6) Yoshino, K.; Kato, T.; Saito, Y.; Shitaba, J.; Hanashima, T.; Nagano, K.; Chiashi, S.; Homma, Y. Temperature Distribution and Thermal Conductivity Measurements of Chirality-Assigned Single-Walled Carbon Nanotubes by Photoluminescence Imaging Spectroscopy. *ACS Omega* **2018**, *3*, 4352−4356.
(7) Mann, D.; Kato, Y. K.; Kinkhabwala, A.; Pop, E.; Cao, J.; Wang, X.; Zhang, L.; Wang, Q.; Guo, J.; Dai, H. Electrically Driven Thermal Light Emission from Individual Single-Walled Carbon Nanotubes. *Nat. Nanotechnol.* **2007**, *2*, 33−38.
(8) Nishihara, T.; Takakura, A.; Miyauchi, Y.; Itami, K. Ultra-Narrow-Band Near-Infrared Thermal Exciton Radiation in Intrinsic One-Dimensional Semiconductors. *Nat. Commun.* **2018**, *9*, 3144.
(9) Yu, M.-F.; Lourie, O.; Dyer, M. J.; Moloni, K.; Kelly, T. F.; Ruoff, R. S. Strength and Breaking Mechanism of Multiwalled Carbon Nanotubes under Tensile Load. *Science* **2000**, *287*, 637−640.
(10) Takakura, A.; Beppu, K.; Nishihara, T.; Fukui, A.; Kozeki, T.; Namazu, T.; Miyauchi, Y.; Itami, K. Strength of Carbon Nanotubes Depends on Their Chemical Structures. *Nat. Commun.* **2019**, *10*, 3040.
(11) Iijima, S.; Ichihashi, T. Single-Shell Carbon Nanotubes of 1-Nm Diameter. *Nature* **1993**, *363*, 603−605.
(12) Saito, R.; Fujita, M.; Dresselhaus, G.; Dresselhaus, M. S. Electronic Structure of Chiral Graphene Tubules. *Appl. Phys. Lett.* **1992**, *60*, 2204−2206.
(13) Wildöer, J. W. G.; Venema, L. C.; Rinzler, A. G.; Smalley, R. E.; Dekker, C. Electronic Structure of Atomically Resolved Carbon Nanotubes. *Nature* **1998**, *391*, 59−62.
(14) Odom, T. W.; Huang, J.-L.; Kim, P.; Lieber, C. M. Atomic Structure and Electronic Properties of Single-Walled Carbon Nanotubes. *Nature* **1998**, *391*, 62−64.
(15) Ando, T. Excitons in Carbon Nanotubes. *J. Phys. Soc. Jpn.* **1997**, *66*, 1066−1073.
(16) Wang, F.; Dukovic, G.; Brus, L. E.; Heinz, T. F. The Optical Resonances in Carbon Nanotubes Arise from Excitons. *Science* **2005**, *308*, 838−841.
(17) Maultzsch, J.; Pomraenke, R.; Reich, S.; Chang, E.; Prezzi, D.; Ruini, A.; Molinari, E.; Strano, M. S.; Thomsen, C.; Lienau, C. Exciton Binding Energies in Carbon Nanotubes from Two-Photon Photoluminescence. *Phys. Rev. B* **2005**, *72*, 241402.
(18) Kataura, H.; Kumazawa, Y.; Maniwa, Y.; Umezu, I.; Suzuki, S.; Ohtsuka, Y.; Achiba, Y. Optical Properties of Single-Wall Carbon Nanotubes. *Synth. Met.* **1999**, *103*, 2555−2558.
(19) O'Connell, M. J.; Bachilo, S. M.; Huffman, C. B.; Moore, V. C.; Strano, M. S.; Haroz, E. H.; Rialon, K. L.; Boul, P. J.; Noon, W. H.; Kittrell, C.; Ma, J.; Hauge, R. H.; Weisman, R. B.; Smalley, R. E. Band Gap Fluorescence from Individual Single-Walled Carbon Nanotubes. *Science* **2002**, *297*, 593−596.
(20) Konabe, S.; Nishihara, T.; Miyauchi, Y. Theory of Exciton Thermal Radiation in Semiconducting Single-Walled Carbon Nanotubes. *Opt. Lett.* **2021**, *46*, 3021−3024.
(21) Nishihara, T.; Takakura, A.; Shimasaki, M.; Matsuda, K.; Tanaka, T.; Kataura, H.; Miyauchi, Y. Empirical Formulation of Broadband Complex Refractive Index Spectra of Single-Chirality Carbon Nanotube Assembly. *Nanophotonics* **2022**, *11*, 1011−1020.

(22) Dumitrica, T.; Hua, M.; Yakobson, B. I. Symmetry-, Time-, and Temperature-Dependent Strength of Carbon Nanotubes. *Proc. Natl. Acad. Sci. U.S.A.* **2006**, *103*, 6105−6109.
(23) Bachilo, S. M.; Balzano, L.; Herrera, J. E.; Pompeo, F.; Resasco, D. E.; Weisman, R. B. Narrow (*n*, *m*)-Distribution of Single-Walled Carbon Nanotubes Grown Using a Solid Supported Catalyst. *J. Am. Chem. Soc.* **2003**, *125*, 11186−11187.
(24) Loebick, C. Z.; Derrouiche, S.; Marinkovic, N.; Wang, C.; Hennrich, F.; Kappes, M. M.; Haller, G. L.; Pfefferle, L. D. Effect of Manganese Addition to the Co-MCM-41 Catalyst in the Selective Synthesis of Single Wall Carbon Nanotubes. *J. Phys. Chem. C* **2009**, *113*, 21611−21620.
(25) Yao, Y.; Feng, C.; Zhang, J.; Liu, Z. "Cloning" of Single-Walled Carbon Nanotubes via Open-End Growth Mechanism. *Nano Lett.* **2009**, *9*, 1673−1677.
(26) Kato, T.; Hatakeyama, R. Direct Growth of Short Single-Walled Carbon Nanotubes with Narrow-Chirality Distribution by Time-Programmed Plasma Chemical Vapor Deposition. *ACS Nano* **2010**, *4*, 7395−7400.
(27) Zhu, Z.; Jiang, H.; Susi, T.; Nasibulin, A. G.; Kauppinen, E. I. The Use of NH_3 to Promote the Production of Large-Diameter Single-Walled Carbon Nanotubes with a Narrow (*n*, *m*) Distribution. *J. Am. Chem. Soc.* **2011**, *133*, 1224−1227.
(28) Liu, J.; Wang, C.; Tu, X.; Liu, B.; Chen, L.; Zheng, M.; Zhou, C. Chirality-Controlled Synthesis of Single-Wall Carbon Nanotubes Using Vapour-Phase Epitaxy. *Nat. Commun.* **2012**, *3*, 1199.
(29) He, M.; Jiang, H.; Liu, B.; Fedotov, P. V.; Chernov, A. I.; Obraztsova, E. D.; Cavalca, F.; Wagner, J. B.; Hansen, T. W.; Anoshkin, I. V.; Obraztsova, E. A.; Belkin, A. V.; Sairanen, E.; Nasibulin, A. G.; Lehtonen, J.; Kauppinen, E. I. Chiral-Selective Growth of Single-Walled Carbon Nanotubes on Lattice-Mismatched Epitaxial Cobalt Nanoparticles. *Sci. Rep.* **2013**, *3*, 1460.
(30) Wang, H.; Ren, F.; Liu, C.; Si, R.; Yu, D.; Pfefferle, L. D.; Haller, G. L.; Chen, Y. $CoSO_4/SiO_2$ Catalyst for Selective Synthesis of (9,8) Single-Walled Carbon Nanotubes: Effect of Catalyst Calcination. *J. Catal.* **2013**, *300*, 91−101.
(31) Yang, F.; Wang, X.; Zhang, D.; Yang, J.; Luo, D.; Xu, Z.; Wei, J.; Wang, J.-Q.; Xu, Z.; Peng, F.; Li, X.; Li, R.; Li, Y.; Li, M.; Bai, X.; Ding, F.; Li, Y. Chirality-Specific Growth of Single-Walled Carbon Nanotubes on Solid Alloy Catalysts. *Nature* **2014**, *510*, 522−524.
(32) Sanchez-Valencia, J. R.; Dienel, T.; Gröning, O.; Shorubalko, I.; Mueller, A.; Jansen, M.; Amsharov, K.; Ruffieux, P.; Fasel, R. Controlled Synthesis of Single-Chirality Carbon Nanotubes. *Nature* **2014**, *512*, 61−64.
(33) Yang, F.; Wang, X.; Zhang, D.; Qi, K.; Yang, J.; Xu, Z.; Li, M.; Zhao, X.; Bai, X.; Li, Y. Growing Zigzag (16,0) Carbon Nanotubes with Structure-Defined Catalysts. *J. Am. Chem. Soc.* **2015**, *137*, 8688−8691.
(34) Ding, F.; Harutyunyan, A. R.; Yakobson, B. I. Dislocation Theory of Chirality-Controlled Nanotube Growth. *Proc. Natl. Acad. Sci. U.S.A.* **2009**, *106*, 2506−2509.
(35) Liu, Y.; Dobrinsky, A.; Yakobson, B. I. Graphene Edge from Armchair to Zigzag: The Origins of Nanotube Chirality? *Phys. Rev. Lett.* **2010**, *105*, 235502.
(36) Artyukhov, V. I.; Penev, E. S.; Yakobson, B. I. Why Nanotubes Grow Chiral. *Nat. Commun.* **2014**, *5*, 4892.
(37) Magnin, Y.; Amara, H.; Ducastelle, F.; Loiseau, A.; Bichara, C. Entropy-Driven Stability of Chiral Single-Walled Carbon Nanotubes. *Science* **2018**, *362*, 212−215.
(38) Bets, K. V.; Penev, E. S.; Yakobson, B. I. Janus Segregation at the Carbon Nanotube-Catalyst Interface. *ACS Nano* **2019**, *13*, 8836−8841.
(39) Förster, G. D.; Swinburne, T. D.; Jiang, H.; Kauppinen, E.; Bichara, C. A Semi-Grand Canonical Kinetic Monte Carlo Study of Single-Walled Carbon Nanotube Growth. *AIP Adv.* **2021**, *11*, 045306.
(40) Rao, R.; Liptak, D.; Cherukuri, T.; Yakobson, B. I.; Maruyama, B. In Situ Evidence for Chirality-Dependent Growth Rates of Individual Carbon Nanotubes. *Nat. Mater.* **2012**, *11*, 213−216.
(41) Otsuka, K.; Ishimaru, R.; Kobayashi, A.; Inoue, T.; Xiang, R.; Chiashi, S.; Kato, Y. K.; Maruyama, S. Universal Map of Gas-Dependent Kinetic Selectivity in Carbon Nanotube Growth. *ACS Nano* **2022**, *16*, 5627−5635.
(42) Liao, Y.; Jiang, H.; Wei, N.; Laiho, P.; Zhang, Q.; Khan, S. A.; Kauppinen, E. I. Direct Synthesis of Colorful Single-Walled Carbon Nanotube Thin Films. *J. Am. Chem. Soc.* **2018**, *140*, 9797−9800.
(43) Wei, N.; Tian, Y.; Liao, Y.; Komatsu, N.; Gao, W.; Lyuleeva-Husemann, A.; Zhang, Q.; Hussain, A.; Ding, E.; Yao, F.; Halme, J.; Liu, K.; Kono, J.; Jiang, H.; Kauppinen, E. I. Colors of Single-Wall Carbon Nanotubes. *Adv. Mater.* **2021**, *33*, 2006395.
(44) Miyauchi, Y.; Chiashi, S.; Murakami, Y.; Hayashida, Y.; Maruyama, S. Fluorescence Spectroscopy of Single-Walled Carbon Nanotubes Synthesized from Alcohol. *Chem. Phys. Lett.* **2004**, *387*, 198−203.
(45) Liu, K.; Hong, X.; Zhou, Q.; Jin, C.; Li, J.; Zhou, W.; Liu, J.; Wang, E.; Zettl, A.; Wang, F. High-Throughput Optical Imaging and Spectroscopy of Individual Carbon Nanotubes in Devices. *Nat. Nanotechnol.* **2013**, *8*, 917−922.
(46) Ishii, A.; Yoshida, M.; Kato, Y. K. Exciton Diffusion, End Quenching, and Exciton-Exciton Annihilation in Individual Air-Suspended Carbon Nanotubes. *Phys. Rev. B* **2015**, *91*, 125427.
(47) Irita, M.; Yamamoto, T.; Homma, Y. Chirality Distributions for Semiconducting Single-Walled Carbon Nanotubes Determined by Photoluminescence Spectroscopy. *Nanomaterials* **2021**, *11*, 2309.
(48) Maruyama, S.; Kojima, R.; Miyauchi, Y.; Chiashi, S.; Kohno, M. Low-Temperature Synthesis of High-Purity Single-Walled Carbon Nanotubes from Alcohol. *Chem. Phys. Lett.* **2002**, *360*, 229−234.
(49) Huang, L.; Cui, X.; White, B.; O'Brien, S. P. Long and Oriented Single-Walled Carbon Nanotubes Grown by Ethanol Chemical Vapor Deposition. *J. Phys. Chem. B* **2004**, *108*, 16451−16456.
(50) Miyauchi, Y.; Zhang, Z.; Takekoshi, M.; Tomio, Y.; Suzuura, H.; Perebeinos, V.; Deshpande, V. V.; Lu, C.; Berciaud, S.; Kim, P.; Hone, J.; Heinz, T. F. Tunable Electronic Correlation Effects in Nanotube-Light Interactions. *Phys. Rev. B* **2015**, *92*, 205407.
(51) Berciaud, S.; Deshpande, V. V.; Caldwell, R.; Miyauchi, Y.; Voisin, C.; Kim, P.; Hone, J.; Heinz, T. F. All-Optical Structure Assignment of Individual Single-Walled Carbon Nanotubes from Rayleigh and Raman Scattering Measurements. *Phys. Status Solidi B* **2012**, *249*, 2436−2441.
(52) Liu, K.; Deslippe, J.; Xiao, F.; Capaz, R. B.; Hong, X.; Aloni, S.; Zettl, A.; Wang, W.; Bai, X.; Louie, S. G.; Wang, E.; Wang, F. An Atlas of Carbon Nanotube Optical Transitions. *Nat. Nanotechnol.* **2012**, *7*, 325−329.
(53) Dukovic, G.; Balaz, M.; Doak, P.; Berova, N. D.; Zheng, M.; Mclean, R. S.; Brus, L. E. Racemic Single-Walled Carbon Nanotubes Exhibit Circular Dichroism When Wrapped with DNA. *J. Am. Chem. Soc.* **2006**, *128*, 9004−9005.
(54) Peng, X.; Komatsu, N.; Bhattacharya, S.; Shimawaki, T.; Aonuma, S.; Kimura, T.; Osuka, A. Optically Active Single-Walled Carbon Nanotubes. *Nat. Nanotechnol.* **2007**, *2*, 361−365.
(55) Wei, X.; Tanaka, T.; Yomogida, Y.; Sato, N.; Saito, R.; Kataura, H. Experimental Determination of Excitonic Band Structures of Single-Walled Carbon Nanotubes Using Circular Dichroism Spectra. *Nat. Commun.* **2016**, *7*, 12899.
(56) Yao, F.; Yu, W.; Liu, C.; Su, Y.; You, Y.; Ma, H.; Qiao, R.; Wu, C.; Ma, C.; Gao, P.; Xiao, F.; Zhao, J.; Bai, X.; Sun, Z.; Maruyama, S.; Wang, F.; Zhang, J.; Liu, K. Complete Structural Characterization of Single Carbon Nanotubes by Rayleigh Scattering Circular Dichroism. *Nat. Nanotechnol.* **2021**, *16*, 1073−1078.

https://doi.org/10.1021/acs.nanolett.2c01473
Nano Lett. 2022, 22, 5818−5824